

Article

Holocene Sedimentary Record and Coastal Evolution in the Makran Subduction Zone (Iran)

Raphaël Normand ^{1,*}, Guy Simpson ¹, Frédéric Herman ², Rabiul Haque Biswas ² and Abbas Bahroudi ³

¹ Department of Earth Sciences, University of Geneva, Rue des Maraîchers 13, 1205 Geneva, Switzerland; guy.simpson@unige.ch

² Institute of Earth Surface Dynamics, Faculty of Geosciences and Environment, University of Lausanne, 1012 Lausanne, Switzerland; frederic.herman@unil.ch (F.H.); rabiulhaque.biswas@unil.ch (R.H.B.)

³ Exploration department, School of Mining Engineering, University of Tehran, Northern Kargaravn, P.O. Box 11365-4563, Tehran 15119-43943, Iran; bahroudi@ut.ac.ir

* Correspondence: raphnormand@gmail.com

Received: 12 April 2019; Accepted: 5 June 2019; Published: 12 June 2019



Abstract: The western Makran coast displays evidence of surface uplift since at least the Late Pleistocene, but it remains uncertain whether this displacement is accommodated by creep on the subduction interface, or in a series of large earthquakes. Here, we address this problem by looking at the short-term (Holocene) history of continental vertical displacements recorded in the geomorphology and sedimentary succession of the Makran beaches. In the region of Chabahar (Southern Iran), we study two bay-beaches through the description, measurement and dating of 13 sedimentary sections with a combination of radiocarbon and Optically Stimulated Luminescence (OSL) dating. Our results show that lagoonal settings dominate the early Holocene of both studied beach sections. A flooding surface associated with the Holocene maximum transgression is followed by a prograding sequence of tidal and beach deposits. Coastal progradation is evidenced in Pozm Bay, where we observe a rapid buildup of the beach ridge succession (3.5 m/years lateral propagation over the last 1950 years). Dating of Beris Beach revealed high rates of uplift, comparable to the rates obtained from the nearby Late Pleistocene marine terraces. A 3150-year-old flooding surface within the sedimentary succession of Chabahar Bay was possibly caused by rapid subsidence during an earthquake. If true, this might indicate that the Western Makran does produce large earthquakes, similar to those that have occurred further east in the Pakistani Makran.

Keywords: Makran; coastal processes; coseismic subsidence; Holocene uplift; headland-bay beach; beach progradation; earthquake

1. Introduction

The Makran coast, in southeastern Iran, sits above oceanic lithosphere of the Arabian plate that is currently subducting northward under Eurasia. The coast has clearly experienced long-term uplift throughout the Late Pleistocene, as evidenced by the presence of emerged sequences of marine terraces, some of which outcrop at more than a hundred meters above present sea-level [1–3]. In eastern Makran (Pakistan), surface uplift of the coastal margin appears to be closely linked with large earthquakes, the last of which was a Mw 8.1 thrust event in 1945 [4,5]. However, in the western segment of the Makran (Iran), there is no obvious historical evidence for large earthquakes in the last 1000 years [6–9]. It is currently unclear whether the lack of seismicity reflects a different mechanical behavior at the subduction interface, or if infrequent large earthquakes occurred in the past and should be expected to happen again [10–12]. Here, we apply some concepts of coastal evolution to the Makran coast, coupled

to observations of the Holocene beach sedimentary record, in order to better understand the nature of vertical motions in the Makran over the last 10,000 years.

Due to their close relation to mean sea level, beaches are prone to record relative sea-level changes related to coseismic vertical motions, as commonly observed in subduction zones [13,14]. Along a coastline experiencing coseismic uplift, a beach staircase profile can develop due to the sudden abandonment of the active ridge during earthquakes [15]. Inversely, in regions experiencing coseismic subsidence, remobilization of the sediments from the destroyed frontal part of the beach into a new active beach ridge situated further landward has been observed to happen in the few years following earthquakes [16]. On the other hand, if the western Makran is behaving aseismically, beach successions are expected to evolve according to continuous rock uplift, along with varying sea level and sediment supply.

Although several studies have considered the long-term uplift recorded by the spectacular Pleistocene marine terraces exposed along the Makran coast [5,17–19], relatively little attention has been focused on the shorter-term record. Paleoseismic studies from the Makran coastline have mainly focused on the tsunami risk associated with megathrust earthquakes within the Makran subduction zone [8,20–25]. A few studies have published paleoseismic observations associated with the Mw 8.1 1945 eastern Makran earthquake [10,26], but geological evidence for older events has rarely been described [27]. Moreover, studies focusing on the beach ridge succession of Chabahar Bay have not considered the potential for coseismic vertical motion [28–30].

In this study, we analyzed the development of two bay-beaches in the Iranian Makran; Chabahar Bay and Beris Bay (Figure 1). We measured 2 and 11 sections, respectively, in these bays in order to understand the history of the beaches using the sedimentary succession of recent deposits. To place time constraints on these sequences, we sampled intervals showing interesting changes in facies for both radiocarbon and optically stimulated luminescence dating (OSL). Furthermore, we visited and sampled the beach ridge succession of Pozm Bay in order to obtain insight on the local coastal progradation. Fluvial sedimentary input was assessed through a study of the watersheds of main tributaries. Our results shed light on the landscape evolution of the region over the Holocene, driven by the interaction between sediment input, eustatic sea level variation and vertical tectonic motion.

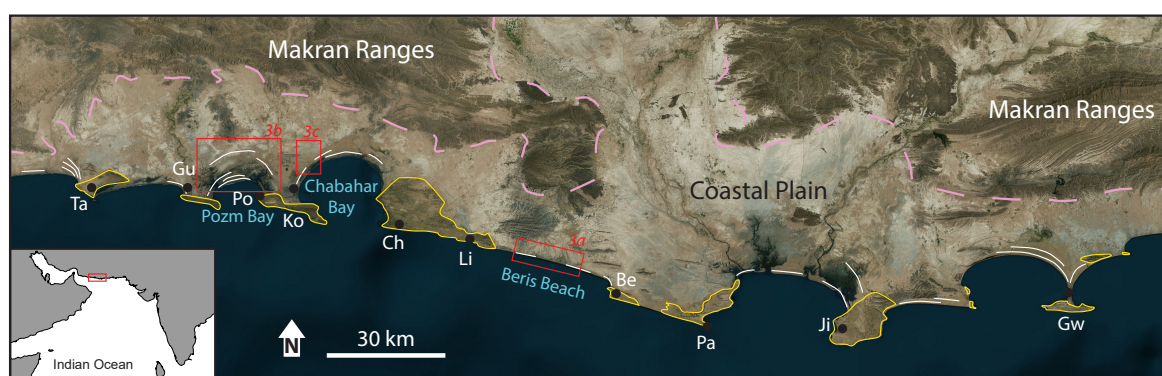


Figure 1. General satellite view of a segment of the Makran coast (image Bing satellite). Pink dashed line: rough delineation of the Makran ranges. White lines: beach ridges. Yellow outlines: protruding headlands. Blue names: studied regions. Red squares: locations of Figure 3a–c. Ta: Tang, Gu: Gurdim, Po: Pozm, Ko: Konarak, Ch: Chabahar, Li: Lipar, Be: Beris, Pa: Pasabander, Ji: Jiwani, Gw: Gwadar.

2. Geological Setting

The Makran subduction zone is the result of the northward subduction of the Arabian plate under Eurasia [4,8,10,31,32]. Although the margin is currently active, as indicated by GPS [33–35] and recently uplifted marine terraces [2,5,18,19,36], seismic activity in the Makran remains relatively low compared to other subduction zones. The eastern segment has experienced several large thrust earthquakes, notably the Mw 8.1 in 1945 [4] and a recent Mw 6.3 event in 2017 [12]. However, the western

segment (the focus of this study) has seemingly not experienced any major thrust earthquake since the historical events of 1008 or 1483 [6,8], whose exact magnitudes, location and focal mechanisms remain controversial [9].

The bedrock geology at the coastal plain [1,2,5,37–43] is dominated by erodible Tertiary marl forming a flat coastal strip (Figure 1). The coastal plain is occasionally punctuated by prominent headlands, whose bedrock geology is dominated by more resistant, late tertiary calcareous sandstones.

The climate in Makran is arid to semi-arid and has been so for at least 5000 years [44–46]. This makes it possible to interpret the Holocene depositional record based on the current coastal setting. The mean annual precipitation is low (127 mm), and occurs mostly during winter [47,48]. Rivers are dry most of the year, but activate during heavy rain episodes resulting in flash flood events inundating the coastal plain and bringing large amounts of sediments to the sea [1,2,39,47,49]. The tide range is micro to mesotidal (1.8–3 m) [18,28], and the current wave regime in Chabahar is mostly towards the NNW, with a maximum significant wave height of 3 m [28,50]. Based on a record spanning 1985–2007, winds come mostly from the south and the west [50,51].

Only a few previous studies have focused on the Holocene coastal depositional record of the Makran [28–30,47]. Radiocarbon dating indicates that the coastal morphologies along the Makran have been developing since the mid-Holocene maximum transgression, around 6000 BP [2,5,10,28–30,47,48,52] (Supplementary Table S1.1). Previous work has shown that the coastline has prograded outwards by up to 20 km since the mid-Holocene maximum transgression [47,53]. Moreover, it has been proposed that the Gurdim and Konarak headlands used to be islands that were progressively attached to the mainland by widening tombolos, evolving into the current omega shaped bay morphology (Figure 1) [2,18,29,49]. The Chabahar Bay-beach has been shown to prograde laterally at about 0.7 m/year between 5500 and 1200 BP, reducing to 0.12 m/year since then [29]. However, dating results from a recent study of the same strandplain imply a much more continuous progradation of 1–2.2 m/year (faster for younger samples) [28].

Signs for the presence of lagoonal systems during the early Holocene in the coastal Pakistani Makran have been observed [47,53]. Some of these ancient lagoons have evolved to low-lying flats, such as those observable west of Pasni and northwest of Gwadar, due to their complete filling by fine alluvial sediments. In fact, we can currently observe that the large active lagoons of the Makran, such as that of Kalat or Miani (Pakistan), host river deltas and will one day be entirely filled.

3. Sea-Level Curve

Knowledge of the sea-level behavior during the Holocene is of utmost importance in order to study the beaches developing during this period. A number of complex sea-level curves have been published from localities around the western Indian Ocean [54], but they are all different in their details and mostly situated too far from the Makran to be relevant to our study. We have focused on the simple Oman Sea curve proposed by Lambeck [55] (Figure 2A). This curve predicts a sea-level rise until 6000 BP, where the sea level stabilized to its current position until today.

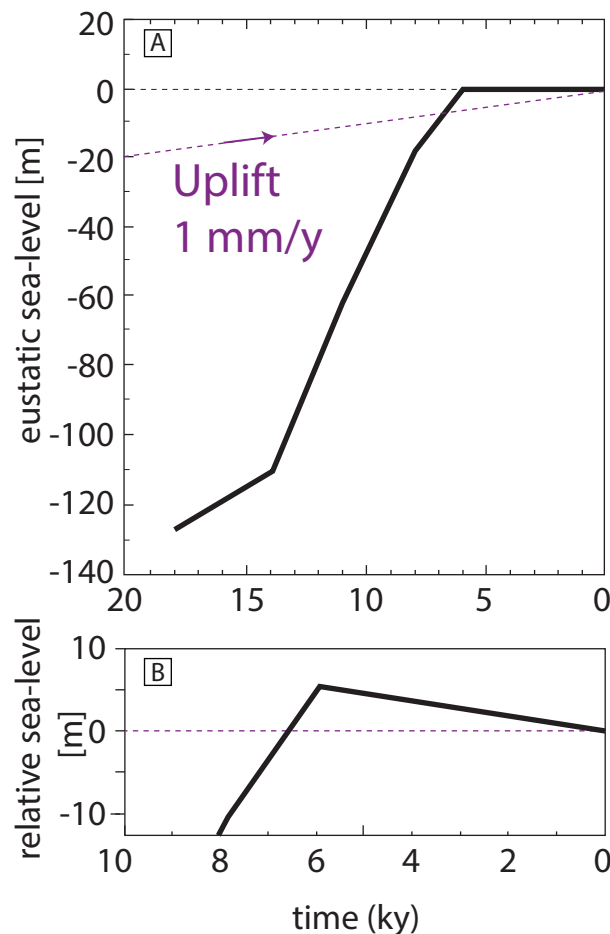


Figure 2. Simplified sea-level curve for the Holocene. (A) Eustatic sea-level curve of Lambeck [55] for the Oman Sea (Muscat). The purple line represents an uplift of 1 mm/year. (B) Holocene relative sea-level changes on a coast uplifting at 1 mm/year, a value considered reliable for the studied segment of the Makran coast [19].

Continental uplift has an impact on the relative sea-level curve and should be taken into consideration. Our limited knowledge of the uplift rate variations during this period creates uncertainty regarding the relative sea-level curve of the Makran. However, the Makran coast has been continuously uplifting during the Late Pleistocene, as shown by the presence of marine terraces [19]. Therefore, the resulting relative sea-level curve should peak at around 6000 ka, hereafter referred to as the mid-Holocene relative highstand, and then slowly fall until the present time. The magnitude of this peak is not well known due to the uncertainties mentioned above (Figure 2B shows an example with 1 mm/year of uplift, consistent with the rates calculated in the Makran [19]).

4. Results

Here, we present the main results of our research on the Holocene beach evolution based on the geomorphological and sedimentological characteristics. Our focus is on three main sites, Beris Beach, Chabahar Bay and Pozm Bay (Figure 3), which we describe separately in the following sections. Details of the methods used are reported in supplementary S2. Dating results are summarized in Tables 1 and 2, and more analytical details are provided in the data repository [56]. The facies description and interpretation of the depositional setting is summarized in Table 3 and detailed in Supplementary Table S1.5. Sedimentary logs, legends and field pictures are compiled in Figures 5 and 7. Additional field pictures can be found in the data repository [56], as referred to in Supplementary Table S1.5.

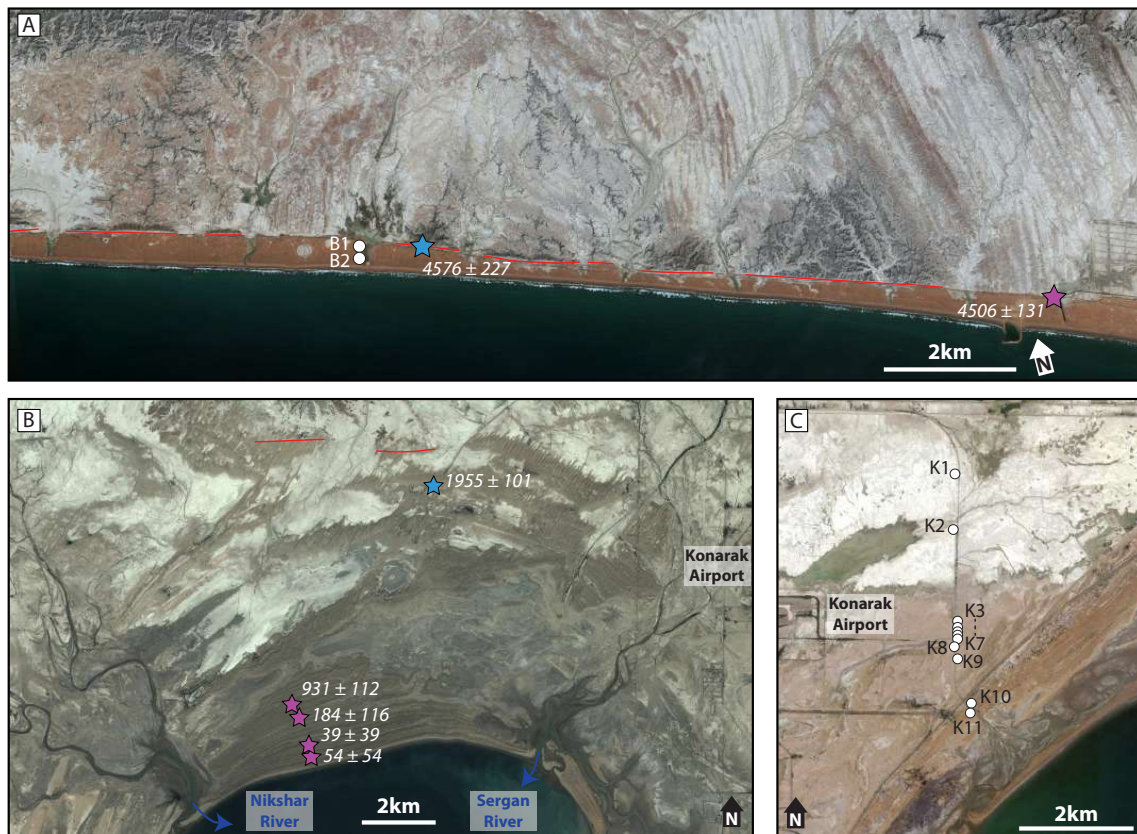


Figure 3. Satellite images of the studied beaches and localization of sampled material and measured logs. Legend: Blue star: OSL sample. Purple star: radiocarbon sample, white circles: stratigraphic logs positions, red lines: paleocliff of the mid-Holocene maximum transgression. (A) Beris Beach. Image from Google Earth (B) Pozm Bay. Image from Bing satellite. (C) Chabahar Bay. Image from Google Earth.

Table 1. Result of radiometric dating. Geolocalisation and more analytical details are in the data repository [56].

Sample	Area	Radiocarbon Age		Comments **	Beach Progradation Rate
		Conventional ± 1σ	Calibrated ± 2σ *		
		BP	Cal BP		m/year
RN15-P3	Pozm Bay	590 ± 30	54 ± 54	290m f.c.	>0.6
RN15-P7	Pozm Bay	490 ± 30	39 ± 39	660m f.c.	>3.3
RN15-P15	Pozm Bay	810 ± 30	184 ± 116	1450m f.c.	>4.8
RN15-P18	Pozm Bay	1620 ± 30	931 ± 112	1840m f.c.	>0.6
RN15-24	Chabahar Bay	4240 ± 30	4010 ± 135	1500m f.c.	0.4
RN16-18	Chabahar Bay	6883 ± 22	7167 ± 101		
RN16-19	Chabahar Bay	3465 ± 20	3041 ± 121		
RN16-29	Chabahar Bay	5969 ± 21	6138 ± 117	In life position	
RN16-34	Chabahar Bay	5903 ± 21	6067 ± 113		
RN16-36	Chabahar Bay	6915 ± 22	7218 ± 84		
RN16-37	Chabahar Bay	5602 ± 21	5743 ± 115		
RN15-89	Beris Beach	4590 ± 30	4506 ± 131	460m f.c.	0.1
RN16-11	Beris Beach	5744 ± 21	5874 ± 107		
RN16-41	Beris Beach	8200 ± 23	8432 ± 88		
RN16-44	Beris Beach	8612 ± 23	8940 46		

* Calibrated using Oxcal 4.2 [57], with the curves IntCal 13 and Marine 13 [58]. Reservoir correction, Delta_R = 236 ± 31 years for Makran, according to the website, <http://calib.org/marine/>. ** f.c.: From the current coastline.

Table 2. Results of OSL dating. Geolocalisation and more analytical details are in the data repository [56].

Area	Location	Sample	Paleodose	N° of	RSD	OD	Env. Dose	Age ± 1σ
			CAM ± 1σ	Aliquots				
			[Gy]	Out of 24	%	%	[Gy/ka]	[yr]
Pozm Bay	7 km from the coastline	RN17-28	2.710 ± 0.121	23	22.3	20	1.386 ± 0.04	1955 ± 101
Chabahar Bay	K3, Above FS	RN17-35	4.489 ± 0.206	24	23.6	21	1.438 ± 0.04	3123 ± 163
Chabahar Bay	K6, Below FS	RN17-36	4.368 ± 0.230	24	21.0	25	1.371 ± 0.03	3187 ± 186
Chabahar Bay	K11	RN17-37	2.287 ± 0.073	24	17.2	15	1.369 ± 0.03	1670 ± 67
Beris Beach	At the base of the cliff	RN17-44	5.929 ± 0.242	24	23.1	19	1.296 ± 0.04	4576 ± 227

Table 3. Short description and interpretation of the facies of Beris and Chabahar Bay cross sections. More details may be found in Supplementary Table S1.5.

Facies	Short Description	Depositional Environment
Beris Beach		
1	Matrix supported, fine-grained laminated deposit	Lagoon
2	Conglomerate, clay matrix	Lagoon with fluvial input
3	Conglomerate, no matrix	Fluvial channel
4	Conglomerate, sandy matrix	Mouth bar
5	Well-sorted sandstone. Cross stratifications	Shoreface
6	Horizontally laminated well sorted sandstone	Beach
Chabahar Bay		
A	Laminated fine-grained deposit, evaporites	Supratidal flats
B	Heavily bioturbated fine-grained deposit	Intertidal ponds
C	Sandy deposits, wavy beddings	Intertidal lagoon
D	Erosive base, channelised, bi-directional cross bedding	Tidal channel
E	Same as D, with occasional <20 cm thick mud drapes	Tidal channel
F	Same as D without the channelised morphology	Intertidal/subtidal
G	Horizontally laminated well sorted sandstone	Beach

4.1. Makran Coastal Evolution

The morphology of the Makran coast is strongly influenced by the spatial distribution of sandstones and marls, which have a marked contrast in resistance (and erodibility) (e.g., [59–61]). Wave action erodes faster through soft marl bedrock than through indurated sandstones, which causes the coastline to develop into deep bays and protruding headlands. Material eroded from headlands, exposed to wave attack, is transported by alongshore currents and preferentially redeposited in embayments, together with continental fluvial input, to form prograding beaches, progressively protecting the bays from coastal retreat [59,61]. The ability of a coastline to either develop a large amplitude, or evolve towards a smooth profile depends on many factors, such as bedrock lithology or wave regime, but it is primarily a function of the sedimentary budget [59,61].

We infer that the sedimentary input supplying the Makran beaches mainly originates from 4 sources (e.g., [45,59,61–64]); (1) alongshore transport of littoral sediments, (2) erosion of nearby headlands, exposed to wave attack, (3) eolian transport and (4) river input. These sources are all linked to climatic conditions, which remained relatively constant in the Makran since the start of the Holocene. However, we observed the presence of abandoned river channels within the low coastal plain (Figure 4A,B) indicating that the Makran Rivers have switched from one bay to another, drastically modifying the sandy fluvial input towards each local bay beach, throughout the Holocene. We gathered information on river watersheds in order to understand where fluvial sediments input the Oman Sea and how fluvial sedimentary input can influence beach progradation. We used a ASTER DEM (30 m), which we analyzed using the Topotoolbox from Matlab [65,66]. The majority of the sand-sized material brought into the Oman Sea by the rivers comes from erosion of the Makran ranges,

northwards of the coastal plain (Figure 4A, brown numbers). In this respect, small watersheds, mostly draining the fine-grained bedrock of the coastal plain, bring little coarse material to build beaches.

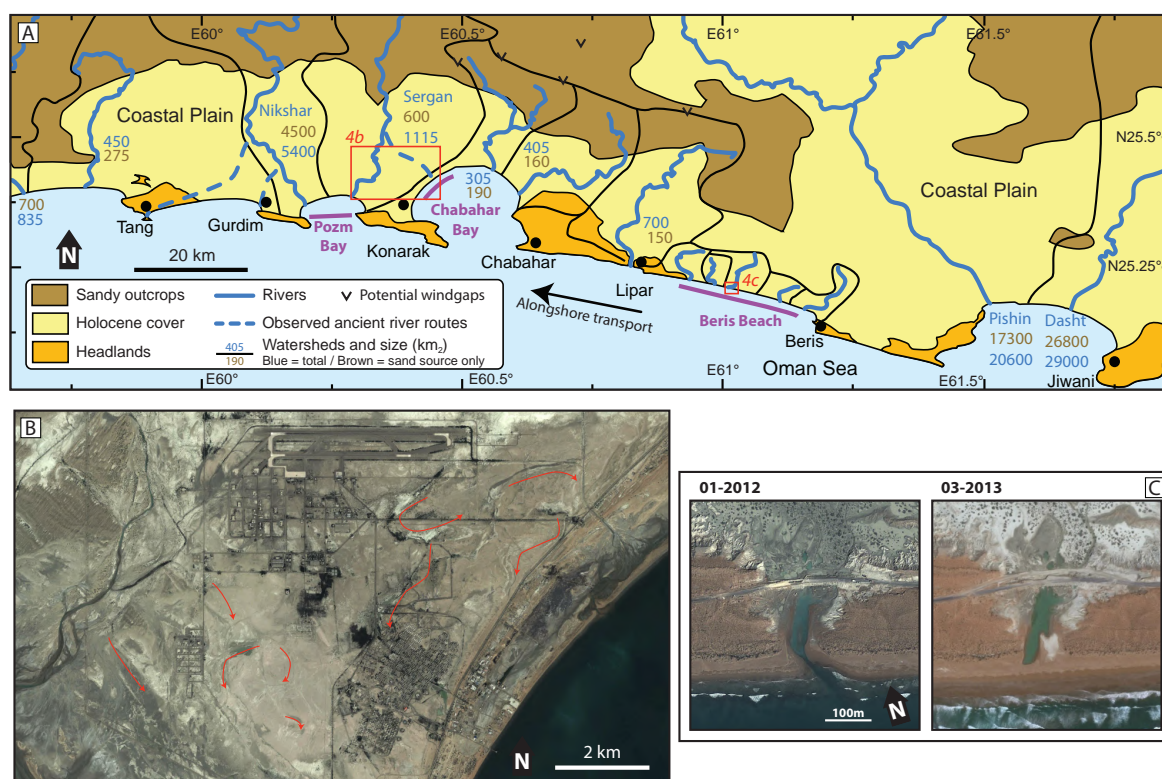


Figure 4. Fluvial input in the Chabahar region. (A) Map of Chabahar region with the watersheds boundaries. Total watershed size is expressed in blue, whereas the watershed area draining hard tertiary bedrock (sand source for beaches) is expressed in brown. Purple = studied regions. (B) Google Earth satellite image near Konarak airport. Abandoned river channels of the Sergan River are visible in the landscape (red arrows). (C) Beach destruction and healing throughout flood events (Beris). N 25.209° E 61.022°. Images from Google Earth.

The presence of headland and bays favors the formation of a concave beach morphology in the shadow zones behind headlands (Figure 1). These crenulated beaches best develop when waves approach the coastline with a steep angle of incidence and are facing towards the main alongshore current direction [67,68]. Most bay-beaches of the western Makran are crenulated, facing towards the west (e.g., Figure 4A), implying a dominant wave direction towards the NW throughout the Late Holocene, as recently measured in Chabahar by [50] (Figure 1, west of Pasabander). Consequently, from this dominant wave direction, alongshore currents are expected to flow from east to west [62]. Interestingly, the crenulated bays of the eastern Makran (Pakistan; Figure 1 east of Jiwani) face in the opposite direction, suggesting a mirrored wave and alongshore regime.

4.2. Beris Beach

Beris Beach is 30 km long and is built on Tertiary marl bedrock between two rocky headlands (Figures 1 and 3A). The high marl cliffs that punctuate the back of this beach (Figure 3A, red line) stand as relicts of the maximum extent of coastal regression that peaked shortly before ~4500 BP, according to our dating results (see below). Since then, relative sea-level fall has favored beach progradation. Its characteristic seaward-concave plan shape (eastern end) is the result of beach building by wave refraction around Beris headland under a NW predominant wave direction [69,70].

At Beris Beach, the oldest beach ridge was sampled at two different locations and dated with two different methods that both yielded an age of ~4500 BP indicating the start of beach deposition at that time. The OSL sample (RN17-44) was sampled at the base of the paleocliff, such that it should correctly estimate the start of beach deposition. Previous dating results from this beach include ages at 3976 ± 29 and 3646 ± 17 BP [48] and 7605 ± 75 BP [10]. The latter, significantly older than other results, is from dating of a lithofaga mollusk found within a boulder that might have been reworked during the transgression.

The beach receives minor fluvial sedimentary input (Figure 4A) and as a result, has remained narrow (250–600m wide, Figure 3A) and has prograded slowly since the mid-Holocene relative highstand (<0.1 m/year). Other sedimentary sources could be alongshore transport (two large watersheds discharge into the nearby Jiwani Bay, Figure 4A) and erosion of the bordering Beris and Lipar headlands, but the distinctive dark orange color of this beach indicates that most of the sand seems to originate from the orange-colored rocks that outcrop north of the beach (Figure 3A). The western part of the beach is nearly linear and is intermittently cross cut by river channels hosting lagoons (Figures 3A and 4C). Looking over a succession of satellite images covering several years, we can see that the river incises through the beach during flash floods, whereas wave action re-builds a continuous beach ridge shortly after the flood events (Figure 4C). The studied section in Beris is situated in one of those incisions and as such, the observed sedimentary facies are greatly influenced by fluvial input and contain a substantial proportion of pebbles.

Beris Beach Sedimentology

B1 and B2 represent, respectively, the proximal and distal parts of the system, which can be inferred by their geographical position as well as by looking at their pebble content (Figure 5). The lower part of the sequence indicates the presence of a lagoon at 8432 ± 88 BP occasionally disturbed by flash flood events (facies 1 and 2). After an erosive surface, the sedimentary succession switches to a facies with a major marine influence (Figure 6). Relative sea-level rise at that time (Figure 2B) explains the presence of this flooding surface. However, we suspect the sample from the sandy layer, dated at 8940 ± 146 BP (i.e., older than the underlying sample, see Figure 5D) to be reworked. During this transgression, the accommodation space is filled with nearshore facies 5, occasionally cross cut by flood conglomerates (facies 4). Conglomerate layers are thicker near the top of section B1, indicating a proximity to the river mouth, where erosion of the wave-built sandy layers occurs during successive floods (Figure 4C, facies 3 in Figure 6). The amount of pebbles decreases upwards and the proportion of sandy matrix increases, probably caused by channel migration. In the distal part of the system (B2), the environment remains marine (dominated by shoreface facies 5) though occasional thin conglomerate layers (facies 4) suggest sporadic fluvial input associated to the more proximal facies seen in B1. Finally, the upper beach facies 6 in B1 and B2 marks the emergence of the succession after the mid-Holocene relative highstand. Since then, the beach has prograded to its current position. This shallowing upwards sedimentary sequence is consistent with the relative sea-level curve (Figure 2B).

4.3. Chabahar Bay

Chabahar Bay is a 20 km wide and 17 km deep omega-shaped bay situated between the two prominent headlands of Chabahar and Konarak (Figure 1). The onshore central part of the bay is occupied by an up to 5 km wide plain of prograding beach ridges flanked by two lagoonal systems. In fact, the Chabahar Bay sedimentary record is dominated by lagoonal, tidal and beach deposits (see Section 4.3.1). We do not observe a paleocliff at the back of the beach; hence, the maximum extent of the Holocene transgression remains unclear. The omega shape of the bay is due to wave diffraction around the two headlands, similar to what can be observed, at a smaller scale, behind human made breakwaters originally separated from the coastline [71]. Hence, it is possible that the rocky headlands of Konarak and Gurdim were detached from the mainland at the start of the Holocene, as has been proposed by other studies [2,18,29,49].

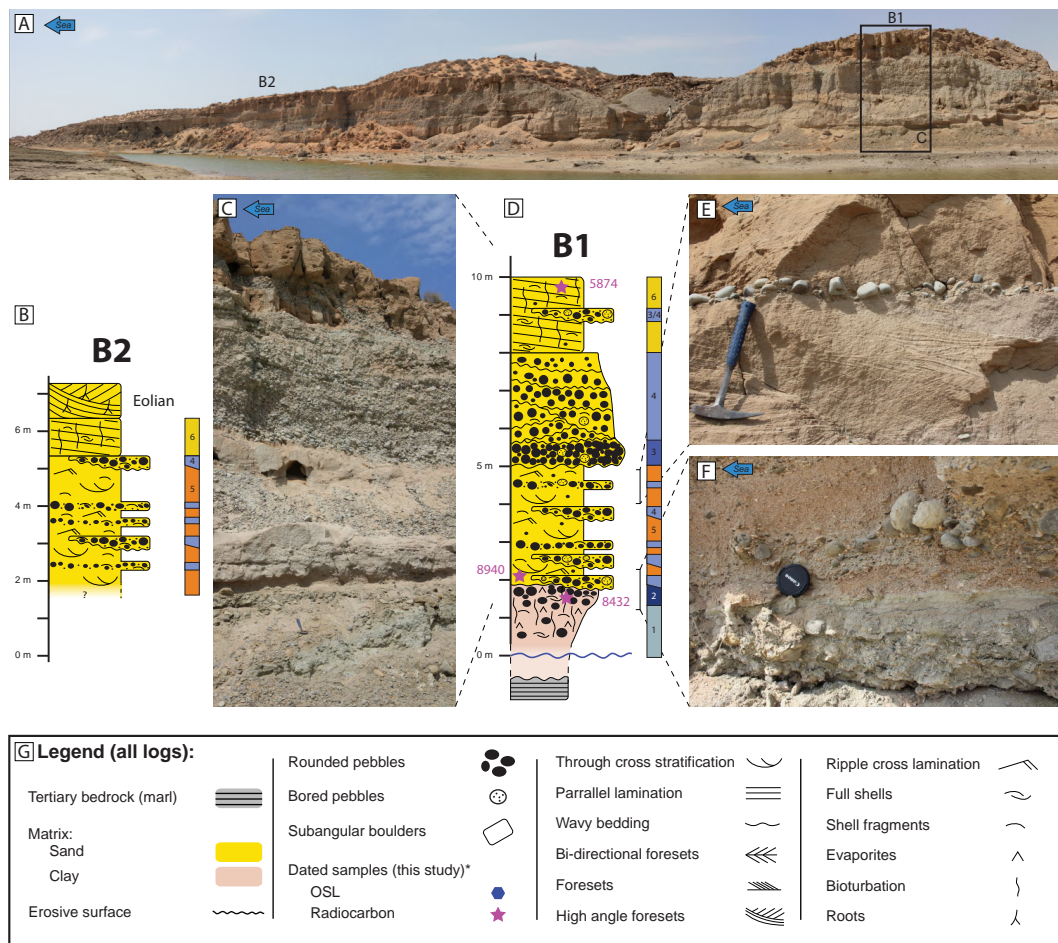


Figure 5. Beris Beach stratigraphic logs. Facies numbering is as reported in Table 3. (A) Beris Beach transect. N 25.219, E 60.985. (B) Log B2. (C) Close up of the transect at the position of log B1 (black square in Figure 5A). (D) Log B1. (E) Close up of facies 5. (F) Close up of the bottom of log B1, the transition from facies 2 to 4-5. (G) Legend for all logs (Figure 5 and Figure 7). *Ages' standard deviations are not reported on the figures but can be seen in Tables 1 and 2. More pictures can be seen in the data repository [56], images C.

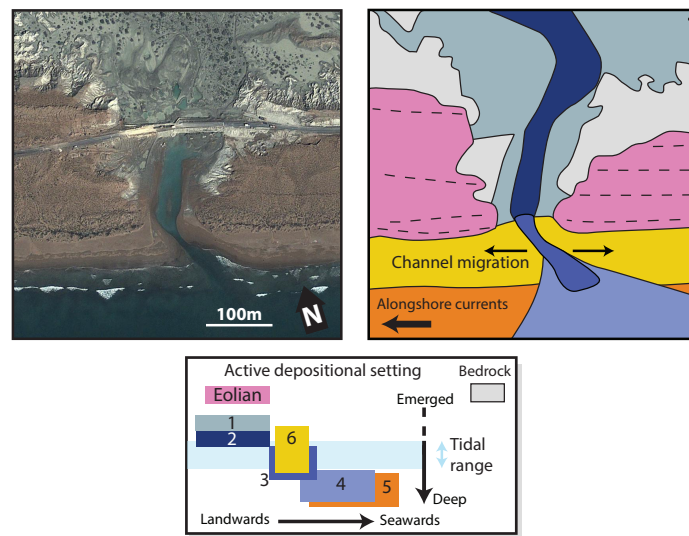


Figure 6. Beris Beach, interpretation of the described facies depositional environment (based on Figure 4C). Black dashed lines: beach ridges. Facies numbering is as reported in Table 3.

Although the presence of this wide strandplain hints towards a high input of sediment, Chabahar Bay currently receives sediments from only two small watersheds (max 500 km²) draining mainly the fine-grained rocks of the coastal plain (Figure 4A). Part of the sand input comes from erosion of the nearby headlands (mainly Chabahar headland, due to its size, upstream position and sandstone dominated bedrock). However, the abandoned river channels observable around Konarak airport (Figure 4B) suggest that the Sergan River used to flow into the Chabahar Bay, nearly tripling its coarse-grained fluvial input (Figure 4A, brown numbers). Results from Gharibreza [29] indicate that beach progradation in Chabahar Bay substantially slowed down at 1200 BP, which might be the moment when the Sergan River diverted towards Pozm Bay. However, recent results of Shah-Hosseini et al. [28] suggest an opposite scenario, where beach progradation increases until today. We also observed potential wind gaps in the Makran Ranges north of Chabahar, hinting towards ancient river routes towards the Chabahar Bay (Figure 4A). However, these routes were probably diverted due to rock uplift, on timescales greater than the Holocene.

4.3.1. Chabahar Bay Sedimentology

We measured eleven logs (Figure 7) along a 4.5 km long man-made trench through the coastal plain near Konarak airport, within Chabahar Bay (Figures 1 and 3C). At this locality, the contact between the Tertiary marl bedrock and the first layers of Holocene fine-grained lagoonal deposits (facies B) was observed ~5 km from the current coastline (K1). This basal lagoonal layer was dated at 6138 ± 117 BP on a shell in life position, indicating deposition of this layer during the mid-Holocene relative highstand. The basal bed is overlain by a thick (up to 3 m observed above the surface) layer of intertidal lagoonal muds, outcropping over a lateral distance exceeding 2.5 km (K2). These deposits become progressively sandier towards the sea and about 3 km from the current coastline they are dominated by sands (facies C) (K4-K8), occasionally cross cut by sandy intertidal channels rich in shell fragments (Facies D, E) (K5-K8). Those intertidal facies are overlain by an extensive layer of laminated muds (facies A), interpreted as supratidal deposits (K3-K6, K8-9). This sequence is typically expected along an emerging coastline experiencing outwards or lateral progradation due to relative sea-level fall and/or high sedimentary input. As new lagoonal settings develop seawards, ancient, inactive intertidal areas become supratidal flats (Figure 8).

A drastic change in facies is observed in the central portion of the sedimentary logs (K3-K9) as the supratidal layered muds of facies A (i.e., deposited above mean sea-level, Figure 8) abruptly transitions to the lower intertidal facies D or F (i.e., deposited below mean sea-level, Figure 8). This succession is visible in most logs (K3-K9) (outlined blue arrow, Figure 7), over a distance of more than 500 m, suggesting it is not a local feature (for example related to channel migration). This sedimentary succession implies the creation of accommodation following the deposition of facies A. Therefore, a relative sea-level rise, or flooding surface, seems to occur within the sedimentary successions, whereas the relative sea-level curve of the Holocene on an uplifting coast would rather be expected to be globally falling (Figure 2B).

We logged two sections toward the seawards end of the section (logs K10 and K11). On the southern flank, the lower part of the K11 log is made of the supratidal muds of facies A, overlain by an erosive surface and the deposition of sandy facies rich in shells interpreted as facies D. This flooding surface can be associated to the mid-Holocene transgression based on our dating results (Figure 7A). The presence of decimetric subangular boulders directly above the erosive surface is attributed to ravinement. The northern section contains low angle lamination of the swash zone, typical of prograding beach ridges (K10).

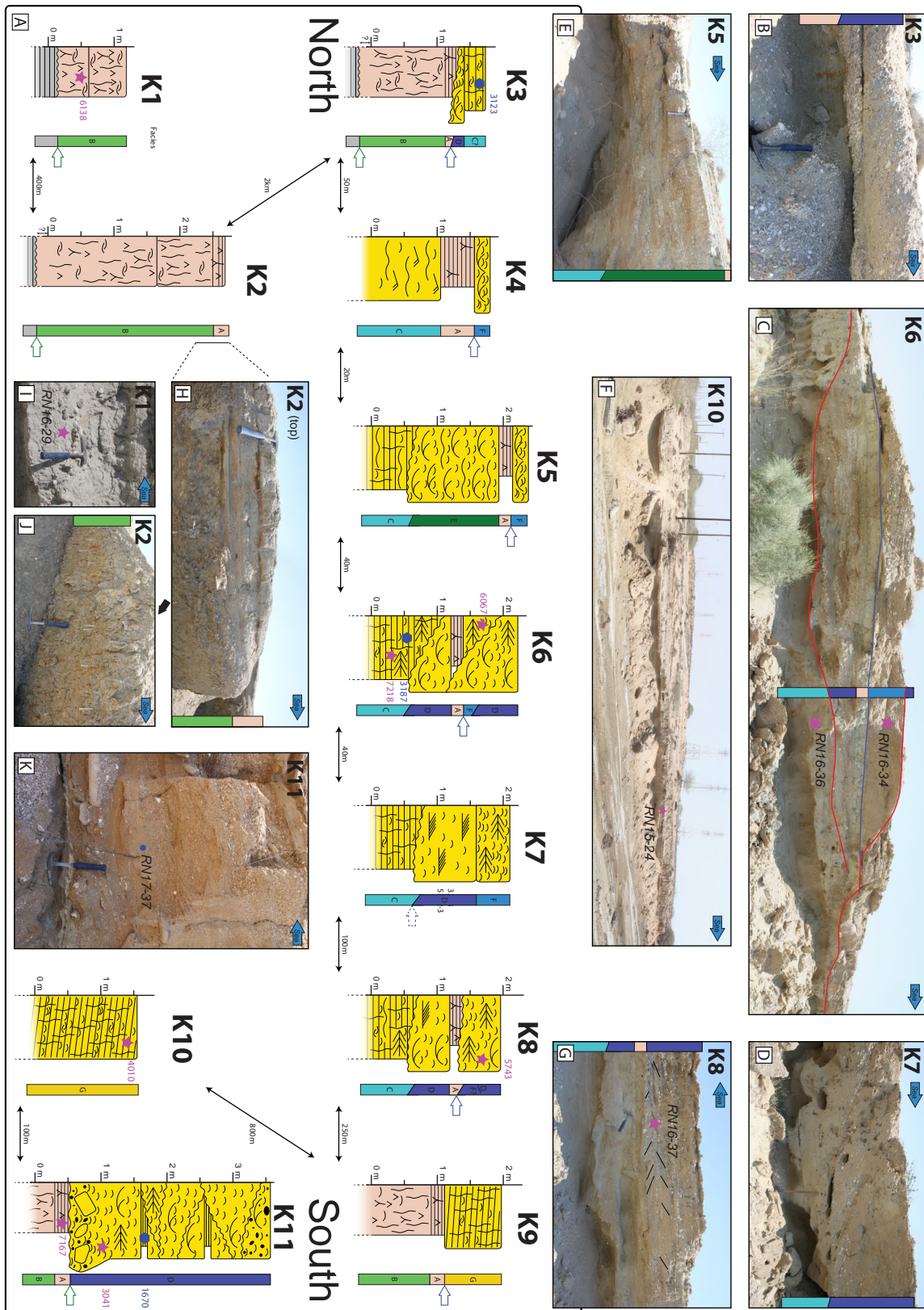


Figure 7. Stratigraphic logs of Konarak Airport section (K1–K11). Facies lettering is as reported in Table 3. Vertical scale is not absolute altitude, but height above the bottom of the channel. Blue outlined arrow: Flooding surface (see Section 4.3.2). Green n arrow: Mid-Holocene transgression. More field pictures can be found in the data repository [56], images B.

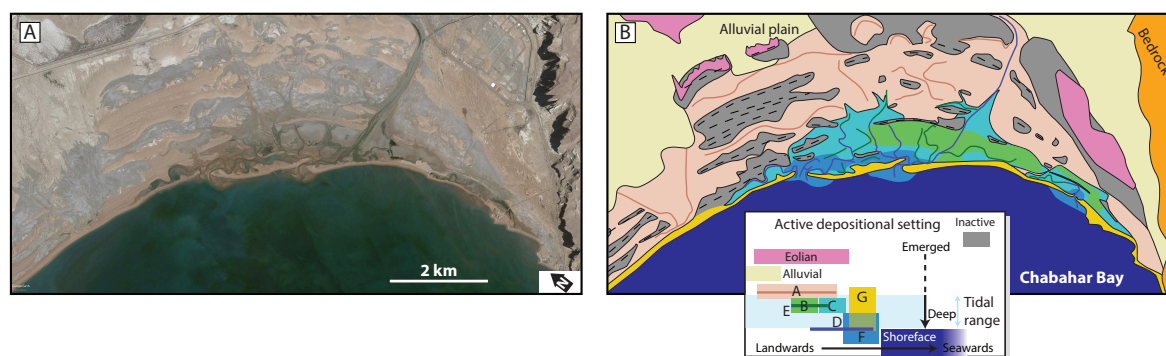


Figure 8. Chabahar Bay depositional setting. Facies lettering is as reported in Table 3. (A) Google Earth satellite image of the eastern part of Chabahar Bay (27/1/2015). N 25.42°, E 60.59°. (B) Interpretation of the described facies depositional environment. Black dashed lines: beach ridges. Colored full lines: tidal channels. Eolian degradation of inactive beach ridges is taking place but is difficult to represent graphically.

4.3.2. Timing of the Flooding Event

We attempted to date the episode of relative sea-level rise observed within the sedimentary logs K3-K9 (outlined blue arrows in Figure 7) in order to understand if this was a slow or fast event, or if it might coincide with the mid-Holocene maximum transgression. Unfortunately, the results are unclear, because OSL and radiocarbon results do not agree with each other (see Figure 7, e.g., log K6). Therefore, we propose two different interpretations based on either method, since combining both leads to ambiguous conclusions.

Based on the radiocarbon results, the lower layer of lagoonal deposits date shortly before the mid-Holocene relative highstand (~7000–6000 BP). At that time, the relative sea level was rising (Figure 2) which seems at odds with the prograding sequence of sediments below the flooding surface (see above). Eventually, the sequence becomes immersed and the coastal regression is expressed in the logs by the flooding surface. After the maximum transgression ~6000 years ago, the relative sea level falls, and the system progrades. Hence, the flooding surface is associated with Early Holocene sea-level rise.

Based on OSL dating, the system postdates the mid-Holocene relative highstand. Samples below and above the flooding surface date at the same age within errors of ~3150 years ago. Therefore, the prograding lagoonal system has been flooded very quickly around 3150 years ago. This rapid relative sea-level rise is at odds with the seemingly steady and undisturbed nature of the sea-level curve at that time (Figure 2).

4.4. Pozm Bay

Pozm Bay is another omega-shaped bay delimited in the east by Konarak and in the west by Gurdim headlands. The size of the bay (12 km wide, 6.5 km deep) is considerably smaller than that of the neighboring Chabahar Bay. However, the paleoclipf, that we observed within the Tertiary marl bedrock, is 9.4 km away from the current coastline (red line, Figure 3C), implying substantial coastal progradation. Two major rivers, the Nikshar and Sergan Rivers, with watersheds of 5400 and 1115 km², respectively, currently discharge into Pozm Bay, though sporadic river avulsion towards the nearby bays has happened throughout the Holocene (Figure 4A,B). The oldest ridges, situated further from the sea, are partially degraded to elongated and NNE directed eolian dunes, as expected from the two main wind directions, coming from the west and south [50]. The lowlands between the oldest ridges (white-covered areas, north of the bay in Figure 3B) are possibly ancient intertidal lagoons. Following flash flood events, these regions of the coastal plain transform into ephemeral ponds where fine-grained alluvial deposit decant. The outer 4 km of the bay hosts a succession of sandy beach ridges, flanked by two active lagoonal systems at the mouths of the rivers (Figures 3B and 4A).

We measured a ~2700 m long topographic profile through the 22 of the southernmost beach ridges of Pozm Bay, with a hand-held GPS (Figure 9, Supplementary Table S1.2–3). The resulting topographical profile shows a succession of topographical ridges that is overall flat. Based on these data, we conclude that the ridges were built by normal beach progradation, driven by high sediment supply and facilitated by relative sea-level fall (e.g., [64,72]). The profile does not indicate a climbing staircase pattern as seen in other subduction zones experiencing repeated episodes of coseismic uplift (e.g., [15]). Some ridges, that are slightly more voluminous (Figure 9A, bolded), could result from extensive sediment rework following a relative sea-level rise, or tsunami (e.g., [16]), but this interpretation remains ambiguous.

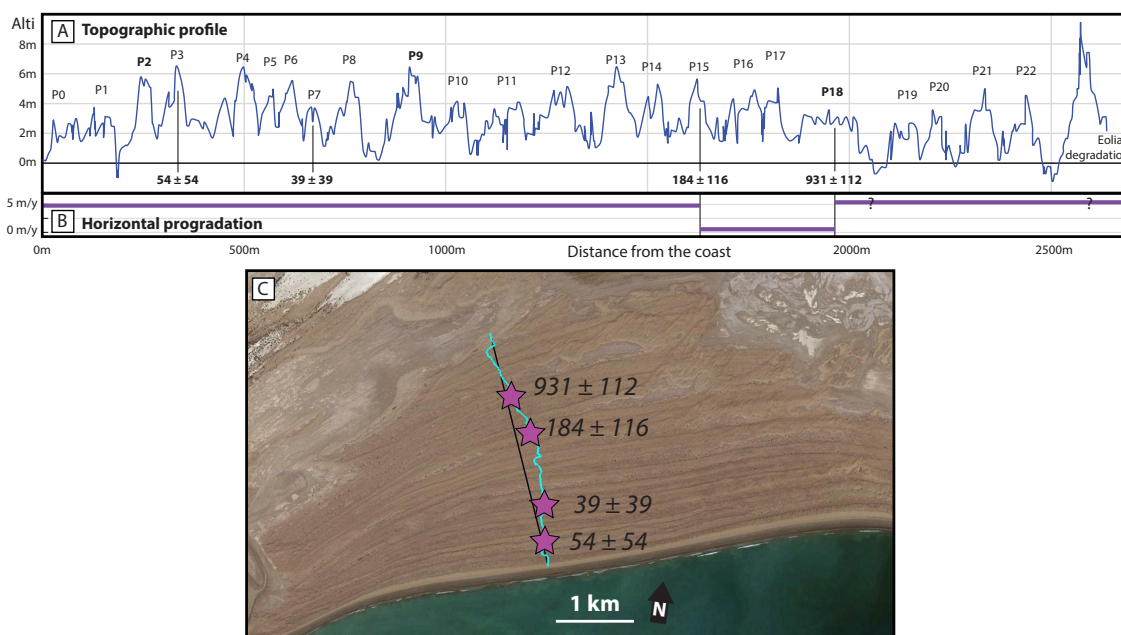


Figure 9. Pozm Bay topographic profile. (A) Topographic profile through the beach ridge succession (see Figure 9C). No obvious step-like topography can be detected. (B) Horizontal progradation rate from dated ridges. (C) Satellite view of Pozm Bay profile (Figure 9A). Image Google Earth, 25.39° N, 60.24° E. The profile is projected on the black line (see Supplementary Table S1.3).

We have dated four shell samples from the beach ridges (from the sea, beach ridge N °3, 7, 15 and 18) (Figure 3B) to better understand the prograding history of the strandplain. Unfortunately, the two first samples yielded very young conventional ages that could not be accurately calibrated. Nonetheless, we know they are recent, (a maximum of several hundred years). The 15th and 18th beach ridges yielded calibrated ages of 184 ± 116 BP and 931 ± 112 BP, respectively (Figure 9). We also sampled one of the oldest beach ridges, close to the observed paleocliff, which yielded an unexpectedly young OSL age of 1955 ± 101 years. Although we aimed to sample beach facies, we do not exclude the possibility that we might have sampled an eolian deposit ([56], image A_1), in which case the OSL age result has to be considered a minimum age for the underlying beach.

Our dating results from the beach ridge succession at Pozm Bay indicate three main facts; (1) According to the OSL results (RN17-28), the active beach ridge was still close to the paleocliff 1955 years ago (i.e., late after the mid-Holocene relative highstand) (Figure 3B, blue star); (2) the recent progradation has been very fast, with a mean value of 5.2 m/year between 1955 ± 101 years and 918 ± 112 years, and a minimum of 4.8 m/year during the last 300 years (Figure 9B); (3) progradation rates seem to have slowed significantly between 931 ± 112 and 184 ± 116 years ago (Figure 9B, beach ridges P18 and P15) (400 m in 747 years, or 0.55 m/year). Nevertheless, a mean progradation rate of 5.2 m/year over a long period of 1955 years is very high and indicates that this OSL age must be considered with caution (see above). The rapid recent (<300 years) beach progradation is probably due

to a local increase in fluvial sedimentary input due to the redirection of one (or both) rivers towards Pozm Bay (Figure 4A,B).

5. Discussion

5.1. Coseismic Signal in Beach Sedimentology?

In Chabahar Bay, we observed a layer of supratidal facies (i.e., deposited above the mean sea-level) overlain by sediments deposited in the lower intertidal zone (i.e., below mean sea-level). This transition is observable in several logs along a distance of more than 500 m; hence, it is not caused by local migration of tidal channels. Although dating using radiocarbon and OSL yield conflicting results (see Section 4.3.1), we favor the OSL data because they directly date sediment deposition and are not affected by reworking issues. These results suggest that Chabahar Bay has undergone an abrupt flooding event 3150 years ago. This rapid flooding event is not consistent with (1) the tectonic uplift experienced by the coast, that tends to emerge the sedimentary system (aside from the discussed transition, the studied vertical succession of facies are generally shallowing upwards), (2) subsidence by sediment compaction, which operate over longer timescales and (3) the form of the eustatic sea-level curve, that is undisturbed since the mid-Holocene transgression (Figure 1). Although there is some uncertainty regarding the details of the local eustatic sea-level curve (see Section 3), the timing and amplitude of this flooding event are too short to be caused by a eustatic sea-level rise. Thus, based on these considerations, we consider it is plausible that the flooding event observed in Chabahar Bay was caused by an earthquake. Although the western segment of the Makran subduction zone (our study area) has not produced a major earthquake in recent times (>500 years), previous work have shown that the potential to produce large earthquakes exist (e.g., [10–12,73]).

If this interpretation is correct, the flooding surface should also be expected within the stratigraphic logs of nearby beaches. Unfortunately, the other sections studied at Beris Beach do not contain sediments as young as this event. Moreover, we find no clear indications for earlier vertical coseismic displacements within the Beris Beach succession. The flooding surface at the base of the Beris Beach sequence is contemporaneous with the Early Holocene eustatic sea-level rise and therefore does not constitute an evidence for coseismic subsidence. In fact, most of the sedimentary facies comprising the Beris section (shoreface facies, Figure 5) do not have a close relation to the sea-level position (Figure 6) and therefore do not record minor relative sea-level changes.

From a study of altitudes of dated beach ridges, Shah-Hosseini et al. [28] constructed a relative sea-level curve of Chabahar Bay. Their curve globally falls over the Holocene, due to an overall uplifting trend of the land [19]. However, the presence of a plateau (due to a lack of data between 3200 and 2000 BP) could be caused by a subsidence event in 3150 BP, followed by uplift. Large boulders along the coast of Oman, interpreted as being displaced by tsunami waves originating in the Makran subduction zone, have been recently dated to 7540 ± 120 cal yr. BP, 1175 ± 115 cal yr. BP and 265 ± 155 cal yr. BP [73]. The possible 3150-year-old event we describe here could complete this record.

In the eastern Makran, Page et al. [5] reported a coseismic uplift of 2 m in Ormara during the 1945 Mw 8.1 earthquake, which seems at odds with the predicted coseismic subsidence that we propose here for the western Makran. However, this difference could be due to the trench-coast distance being smaller in the eastern than in the western Makran (~75 km in Ormara, ~130km in Chabahar), which would favor coseismic uplift in the east and coseismic subsidence in the west (e.g., Figure 10A, green line, [74–77]).

5.2. Holocene Uplift Rates

Rock uplift rates are of interest to try to understand the seismic behavior of the region. Short-term uplift rates, based on Holocene dates, have been observed to be very different (most of the times, higher) from those obtained on longer time scales (usually from Pleistocene marine terraces) [78–80]. On a time scale of a few thousand years, coseismic and interseismic vertical movements are a major component

of the total vertical displacement [81]. Hence, in this context, the timing of sample deposition and present position within the seismic cycle is expected to be an important factor influencing short-term uplift rates, if the margin does indeed experience large earthquakes (see Figure 10).

Uplift calculations based on Holocene samples have been attempted by previous authors [5,10,28, 29,48] and are also presented here based on our results (Table 4). Holocene mean uplift rates from near the middle of Beris Beach are very high, varying between 2.9 and 3.75 mm/year. These values fit quite well with the Late Pleistocene trends obtained from marine terraces [19], where long-term uplift rates along Beris Beach increase from from 1 to 5 mm/year going from west to east. Note that the uncertainties regarding the Pleistocene uplift trend along Beris Beach are high due to local lack of data [19], which makes comparison to Holocene rates dubious. However, the fast Holocene uplift rates obtained here emphasize the highly active nature of the tectonics in this region.

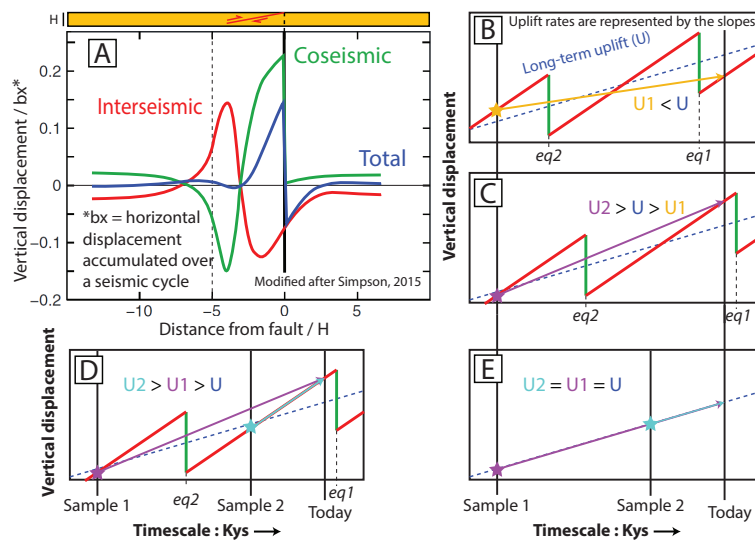


Figure 10. Scenarios of vertical displacements on a seismically active subduction zone. eq: earthquake. (A) Vertical deformation distribution based on a viscoelastic model of elastic rebound for a thrust earthquake [81]. Our example scenarios of Figure 10B–D are at $\sim -5H$ from the trench (dashed black line), where coseismic subsidence and interseismic uplift occurs. Red and green lines represent the interseismic and coseismic movement of the continent (overriding plate of a subduction thrust), respectively. (B,C) show two different scenarios, where the timing of sample deposition and present day position within the seismic cycle affect the resulting short-term uplift rates. Do fast Holocene rates calculated for the Makran imply an upcoming coseismic subsidence earthquake (like in Figure 10C)? (D) Example showing how samples with different ages and having different uplift rates suggest a non-linear history of vertical displacements. (E) Example where continuous deformation happens without coseismic vertical displacements, U_1 , U_2 and U are expected to be equal.

Table 4. Holocene uplift rates. Uplift rates based on lagoonal deposits are more precise than those based on beach deposits. More details in Supplementary Text S2 and Table S1.4.

Area	Sample	Deposits	Age $\pm 2\sigma$	Mean Uplift Rate Since Age	Pleistocene Uplift Rate [19]
			[years]	[mm/year]	[mm/year]
Chabahar Bay	RN15-24	Beach	4010 \pm 135	1.29 \pm 0.9	\sim 0.6
	RN16-18	Lagoon	7167 \pm 101	1.88 \pm 0.2	\sim 0.6
	RN16-29	Lagoon	6138 \pm 117	1.38 \pm 0.4	\sim 0.6
Beris Beach	RN15-89	Beach	4506 \pm 131	2.92 \pm 1.2	1 to 4
	RN16-41	Lagoon	8432 \pm 88	3.38 \pm 0.2	1 to 4
	RN17-44 (OSL)	Beach	4576 \pm 454	3.75 \pm 1.8	1 to 4

In Chabahar Bay, previous uplift results vary substantially, ranging from 0.7 to 4.75 mm/year [28,29]. Our results in the western Chabahar Bay vary between 1.3 and 1.9 mm/year. Both our and previous results are higher than the predicted long-term trend of ~0.6 mm/year obtained from the Konarak marine terraces situated 10 km southwards [19].

Holocene uplift rates obtained from lagoonal and beach deposits in Chabahar Bay are much higher than Pleistocene uplift rates obtained from marine terraces. Moreover, within the same beach, calculated uplift rates differ, depending on the age of the considered sample (i.e., the time considered for averaging the uplift rate) (Table 4) (see Figure 10D). This indicates a complex history of vertical movements on time scales of less than several millennia, possibly related to coseismic movements. We do not currently have sufficient data to provide a clearer picture of the vertical motion of this region over the Holocene. However, the fact that short-term and long-term uplift trends are different (e.g., Figure 10B,C) might indicate that the short-term uplift history of the Chabahar region is strongly influenced by large, infrequent earthquakes.

6. Conclusions

In this study, we have presented sedimentological data along with dating to show the evolution of the coastal Makran in Iran during the Holocene. Results from two studied beach sections indicate that since 8400 BP, some regions of the coastal Makran were already occupied by the sea. Coastal lagoons were progressively submerged with time until the maximum Holocene transgression. Since then, deposition was dominated by prograding sequences of tidal and beach deposits. Variation in the rate of coastal progradation during the Late Holocene seems to be linked to the migration of fluvial sedimentary input from one bay to another.

Our observations are in line with what might be expected on an uplifting coast. However, a flooding surface divides the Late Holocene sedimentary succession of Chabahar Bay. This rapid flooding event, dated at 3150 years BP from two (underlying and overlying) OSL results, is attributed to coastal subsidence caused by a large subduction earthquake. Additionally, short-term uplift rates, obtained from our Holocene samples, vary depending on the timescale considered. This might indicate a complex history of vertical displacements, possibly linked to coseismic movements.

Supplementary Materials: The following are available online at <http://www.mdpi.com/2571-550X/2/2/21/s1>, Table S1: Published Makran beach dating results, Pozm Bay GPS data, Uplift rate calculation method and observed facies descriptions. Text S2: Description of the methods used in this paper: Fieldwork approach, radiocarbon dating, OSL dating, calculation of uplift rates. Data repository: [56], field pictures, radiocarbon dating analytical details, OSL dating analytical details.

Author Contributions: Conceptualization, R.N. and G.S.; Formal analysis, R.N., F.H. and R.H.B.; Funding acquisition, G.S.; Investigation, R.N., G.S., F.H., R.H.B. and A.B.; Methodology, R.N.; Project administration, G.S. and A.B.; Resources, F.H. and R.H.B.; Visualization, R.N.; Writing—original draft, R.N.; Writing—review & editing, R.N., G.S., F.H., R.H.B. and A.B.

Funding: This work was funded by the Swiss National Science Foundation, project n°200021_155904.

Acknowledgments: We are grateful to Reza Ensani, Feisal Arjomandi, Nurrudin Mazarzezi, Yousef Adeeb and Gholamreza Hosseinyar for helping us with logistics in Iran and accompanying us in the field. We also thank Irka Hajdas for analytical assistance with radiocarbon dating, Agathe Martignier for SEM, Annette Süssenberger and Emanuelle Ricchi for XRD analysis.

Conflicts of Interest: The authors declare no conflict of interest.

References

1. Falcon, N.L. Raised beaches and terraces of the Iranian Makran coast. *Geogr. J.* **1947**, *109*, 149–151.
2. Snead, R.J. Recent Morphological changes along the coast of West Pakistan. *Ann. Assoc. Am. Geogr.* **1967**, *57*, 550–565. [[CrossRef](#)]
3. Reyss, J.L.; Pirazzoli, P.A.; Haghypour, A.; Hatté, C.; Fontugne, M. Quaternary marine terraces and tectonic uplift rates on the south coast of Iran. *Geol. Soc. Lond. Spec. Publ.* **1998**, *146*, 225–237. [[CrossRef](#)]

4. Byrne, D.E.; Sykes, L.R.; Davis, D.M. Great Thrust Earthquakes and Aseismic Slip Along the Plate Boundary of the Makran Subduction Zone. *J. Geophys. Res. Earth* **1992**, *97*, 449–478. [[CrossRef](#)]
5. Page, W.D.; Alt, J.N.; Cluff, L.S.; Plafker, G. Evidence for the recurrence of large-magnitude earthquake along the Makran coast of Iran and Pakistan. *Tectonophysics* **1979**, *52*, 533–547. [[CrossRef](#)]
6. Ambraseys, N.N.; Melville, C.P. *A History of Persian Earthquakes*; Cambridge University Press: Cambridge, UK, 1982. [[CrossRef](#)]
7. Quittmeyer, R.C.; Jacob, K.H. Historical and Modern seismicity of Pakistan, Afghanistan, Northwestern India, and Southeastern Iran. *Bull. Seismol. Soc. Am.* **1979**, *69*, 773–823.
8. Heidarzadeh, M.; Pirooz, M.D.; Zaker, N.H.; Yalciner, A.C.; Mokhtari, M.; Esmaily, A. Historical tsunami in the Makran Subduction Zone off the southern coasts of Iran and Pakistan and results of numerical modeling. *Ocean Eng.* **2008**, *35*, 774–786. [[CrossRef](#)]
9. Musson, R.M.W. Subduction in the Western Makran: The historian's contribution. *J. Geol. Soc. Lond.* **2009**, *166*, 387–391. [[CrossRef](#)]
10. Rajendran, C.P.; Rajendran, K.; Shah-hosseini, M.; Beni, A.N.; Nautiyal, C.M.; Andrews, R. The hazard potential of the western segment of the Makran subduction zone, northern Arabian Sea. *Nat. Hazards* **2013**, *65*, 219–239. [[CrossRef](#)]
11. Smith, G.L.; McNeill, L.C.; Wang, K.; He, J.; Henstock, T.J. Thermal structure and megathrust seismogenic potential of the Makran subduction zone. *Geophys. Res. Lett.* **2013**, *40*, 1528–1533. [[CrossRef](#)]
12. Penney, C.; Tavakoli, F.; Saadat, A.; Nankali, H.R.; Sedighi, M.; Khorrani, F.; Sobouti, F.; Rafi, Z.; Copley, A.; Jackson, J.; et al. Megathrust and accretionary wedge properties and behaviour in the Makran subduction zone. *Geophys. J. Int.* **2017**, *209*, 1800–1830. [[CrossRef](#)]
13. Darwin, C. *Geological Observations on South America*; Cambridge University Press: Cambridge, UK, 1846. [[CrossRef](#)]
14. Atwater, B.F.; Musumi-Rokkaku, S.; Satake, K.; Tsuji, Y.; Ueda, K.; Yamaguchi, D.K. *The Orphan Tsunami of 1700—Japanese Clues to a Parent Earthquake in North America*; U.S. Geological Survey Professional Paper 1707; University of Washington Press: Seattle, WA, USA, 2005. [[CrossRef](#)]
15. McSaveney, M.J.; Graham, I.J.; Begg, J.G.; Beu, A.G.; Hull, A.G.; Kim, K.; Zondervan, A. Late Holocene uplift of beach ridges at Turakirae Head, south Wellington coast, New Zealand. *N. Z. J. Geol. Geophys.* **2006**, *49*, 337–358. [[CrossRef](#)]
16. Monecke, K.; Templeton, C.K.; Finger, W.; Houston, B.; Luthi, S.; Mcadoo, B.G.; Meilianda, E.; Storms, J.E.A.; Walstra, D.; Amna, R.; et al. Beach ridge patterns in West Aceh, Indonesia, and their response to large earthquakes along the northern Sunda trench. *Quat. Sci. Rev.* **2015**, *113*, 159–170. [[CrossRef](#)]
17. Vita-Finzi, C. Recent coastal deformation near the Strait of Hormuz. *Proc. R. Soc. Lond.* **1982**, *382*, 441–457. [[CrossRef](#)]
18. Snead, R.J. Uplifted Marine Terraces along the Makran coast of Pakistan and Iran. In *Himalaya to the Sea*; Shroder, J.F.J., Ed.; Routledge: London, UK, 1993; pp. 327–362.
19. Normand, R.; Simpson, G.; Herman, F.; Biswas, R.H.; Bahroudi, A.; Schneider, B. Dating and morpho-stratigraphy of uplifted marine terraces in the Makran subduction zone (Iran). *Earth Surf. Dyn.* **2019**, *7*, 321–344. [[CrossRef](#)]
20. Pararas-Carayannis, G. The Potential of Tsunami Generation along the Makran Subduction. *Sci. Tsunami Hazards* **2006**, *24*, 358–384.
21. Hafeez, H. The potential of tsunami generation along Karachi and the Makran coast of Pakistan. *Pak. J. Meteorol.* **2007**, *4*, 25–40. [[CrossRef](#)]
22. Rajendran, C.P.; Ramanamurthy, M.V.; Reddy, N.T.; Rajendran, K. Hazard implications of the late arrival of the 1945 Makran tsunami. *Curr. Sci.* **2008**, *95*, 1739–1743.
23. Heidarzadeh, M.; Kijko, A. A probabilistic tsunami hazard assessment for the Makran subduction zone at the northwestern Indian Ocean. *Nat. Hazards* **2011**, *56*, 577–593. [[CrossRef](#)]
24. Schneider, B.; Hoffmann, G.; Reicherter, K. Scenario-based tsunami risk assessment using a static flooding approach and high-resolution digital elevation data: An example from Muscat in Oman. *Glob. Planet. Chang.* **2016**, *139*, 183–194. [[CrossRef](#)]
25. Hoffmann, G.; Reicherter, K.; Wiatr, T.; Grützner, C.; Rausch, T. Block and boulder accumulations along the coastline between Fins and Sur (Sultanate of Oman): Tsunamigenic remains? *Nat. Hazards* **2013**, *65*, 851–873. [[CrossRef](#)]

26. Donato, S.V.; Reinhardt, E.G.; Boyce, J.I.; Pilarczyk, J.E.; Jupp, B.P. Particle-size distribution of inferred tsunami deposits in Sur Lagoon, Sultanate of Oman. *Mar. Geol.* **2009**, *257*, 54–64. [[CrossRef](#)]
27. Shah-Hosseini, M.; Morhange, C.; Naderi Beni, A.; Marriner, N.; Lahijani, H.; Hamzeh, M.; Sabatier, F. Coastal boulders as evidence for high-energy waves on the Iranian coast of Makran. *Mar. Geol.* **2011**, *290*, 17–28. [[CrossRef](#)]
28. Shah-Hosseini, M.; Ghanavati, E.; Morhange, C.; Naderi Beni, A.; Lahijani, H.A.; Hamzeh, M.A. The evolution of Chabahar beach ridge system in SE Iran in response to Holocene relative sea level changes. *Geomorphology* **2018**, *318*, 139–147. [[CrossRef](#)]
29. Gharibreza, M. Evolutionary trend of paleoshorelines in the Coastal Makran zone (Southeast Iran) since the mid-Holocene. *Quat. Int.* **2016**, *392*, 203–212. [[CrossRef](#)]
30. Gharibreza, M.R.; Motamed, A. Late Quaternary Paleoshorelines and Sedimentary Sequences in Chabahar Bay (Southeast of Iran). *J. Coast. Res.* **2006**, *226*, 1499–1504. [[CrossRef](#)]
31. Zare, M.; Amini, H.; Yazdi, P.; Sesetyan, K.; Demircioglu, M.B.; Kalafat, D.; Erdik, M.; Giardini, D.; Khan, M.A.; Tsereteli, N. Recent developments of the Middle East catalog. *J. Seismol.* **2014**, *18*, 749–772. [[CrossRef](#)]
32. Smith, G.; McNeill, L.; Henstock, I.J.; Bull, J. The structure and fault activity of the Makran accretionary prism. *J. Geophys. Res. Solid Earth* **2012**, *117*, 1–17. [[CrossRef](#)]
33. Vernant, P.; Nilforoushan, F.; Hatzfeld, D.; Abbassi, M.R.; Vigny, C.; Masson, F.; Nankali, H.; Martinod, J.; Ashtiani, A.; Bayer, R.; et al. Present-day crustal deformation and plate kinematics in the Middle East constrained by GPS measurements in Iran and northern Oman. *Geophys. J. Int.* **2004**, *157*, 381–398. [[CrossRef](#)]
34. Masson, F.; Anvari, M.; Djamour, Y.; Walpersdorf, A.; Tavakoli, F.; Daignières, M.; Nankali, H.; Van Gorp, S. Large-scale velocity field and strain tensor in Iran inferred from GPS measurements: New insight for the present-day deformation pattern within NE Iran. *Geophys. J. Int.* **2007**, *170*, 436–440. [[CrossRef](#)]
35. Khan, M.A.; Bendick, R.; Bhat, M.I.; Bilham, R.; Kakar, D.M.; Khan, S.F.; Lodi, S.H.; Qazi, M.S.; Singh, B.; Szeliga, W.; et al. Preliminary geodetic constraints on plate boundary deformation on the western edge of the Indian plate from TriGGnet (Tri-University GPS Geodesy Network). *J. Himal. Earth Sci.* **2008**, *41*, 71–87.
36. Vita-Finzi, C. Neotectonics in the Arabian Sea coasts. *Geol. Soc. Lond. Spec. Publ.* **2002**, *195*, 87–96. [[CrossRef](#)]
37. Burg, J.-P.; Dolati, A.; Bernoulli, D.; Smit, J. Structural style of the Makran Tertiary accretionary complex in SE-Iran. In *Lithosphere Dynamics and Sedimentary Basins: The Arabian Plate and Analogues*; Al Hosani, K., Roure, F., Ellison, R., Lokier, S., Eds.; Springer: Berlin, Germany, 2013; pp. 239–259.
38. McCall, G.J.H. A summary of the geology of the Iranian Makran. *Geol. Soc. Lond. Spec. Publ.* **2002**, *195*, 147–204. [[CrossRef](#)]
39. Harrison, J.V. Coastal Makran: Discussion. *Geogr. J.* **1941**, *97*, 1–15. [[CrossRef](#)]
40. Harms, J.C.; Cappel, H.N.; Francis, D.C. The Makran Coast of Pakistan: It's Stratigraphy and Hydrocarbon Potential. In *Marine Geology and Oceanography of Arabian Sea and Coastal Pakistan*; Haq, B.U., Milliman, J.D., Eds.; Van Nostrand Reinhold Company Inc.: New York, NY, USA, 1984; pp. 3–26.
41. Ghorashi, M. Late Cainozoic faulting in S.E. Iran. Ph.D. Thesis, University College London, London, UK, 1978.
42. Blanford, W.T. Note on the geological formations seen along the coasts of Bilúchistán and Persia from Karáchi to the head of the Persian Gulf, and on some of the Gulf Islands. *Rec. Geol. Surv. India* **1872**, *5*, 41–45.
43. Stiffe, A.W. On the Mud-craters and Geological Structure of the Mekran Coast. *Q. J. Geol. Soc. Lond.* **1874**, *30*, 50–53. [[CrossRef](#)]
44. Ivory, S.J.; Lézine, A.M. Climate and environmental change at the end of the Holocene Humid Period: A pollen record off Pakistan. *C. R. Geosci.* **2009**, *341*, 760–769. [[CrossRef](#)]
45. Prins, M.A.; Postma, G.; Cleveringa, J.; Cramp, A.; Kenyon, N.H. Controls on terrigenous sediment supply to the Arabian Sea during the late quaternary: The Indus fan. *Mar. Geol.* **2000**, *169*, 327–349. [[CrossRef](#)]
46. Bourget, J.; Zaragosi, S.; Ellouz-Zimmermann, S.; Ducassou, E.; Prins, M.A.; Garlan, T.; Lanfumeu, V.; Schneider, J.L.; Rouillard, P.; Giraudeau, J. Highstand vs. lowstand turbidite system growth in the Makran active margin: Imprints of high-frequency external controls on sediment delivery mechanisms to deep water systems. *Mar. Geol.* **2010**, *274*, 187–208. [[CrossRef](#)]
47. Sanlaville, P.; Besenval, R.; Evin, J.; Prieur, A. Evolution de la région littorale du Makran pakistanaise à l'Holocène. *Paléorient* **1991**, *17*, 3–18. [[CrossRef](#)]
48. Haghypour, N.; Burg, J.P.; Ivy-Ochs, S.; Hajdas, I.; Kubik, P.; Christl, M. Correlation of fluvial terraces and temporal steady-state incision on the onshore Makran accretionary wedge in southeastern Iran: Insight

- from channel profiles and ¹⁰Be exposure dating of strath terraces. *Bull. Geol. Soc. Am.* **2014**, *127*, 560–583. [[CrossRef](#)]
49. Little, R.D. Terraces of the Makran Coast of Iran and Parts of West Pakistan. Ph.D. Thesis, University of Southern California, Los Angeles, CA, USA, 1972.
 50. Saket, A.; Etemad-shahidi, A. Wave energy potential along the northern coasts of the Gulf of Oman, Iran. *Renew. Energy* **2012**, *40*, 90–97. [[CrossRef](#)]
 51. Saket, A.; Etemad-shahidi, A.; Moeini, M.H. Evaluation of ECMWF wind data for wave hindcast in Chabahar zone. *J. Coast. Res.* **2013**, 380–385. [[CrossRef](#)]
 52. Vita-Finzi, C. ¹⁴C Dating of recent crustal movements in the Persian Gulf and Iranian Makran. *Radiocarbon* **1980**, *22*, 763–773. [[CrossRef](#)]
 53. Sanlaville, P.; Dalongeville, R. L'évolution des espaces littoraux du golfe Persique et du golfe d'Oman depuis la phase finale de la transgression post-glaciaire. *Paléorient* **2005**, *31*, 9–26. [[CrossRef](#)]
 54. Pirazzoli, P.A. *World Atlas of Holocene Sea-Level Changes*; Elsevier B.V.: Amsterdam, The Netherlands, 1991.
 55. Lambeck, K. Shoreline reconstructions for the Persian Gulf since the last glacial maximum. *Earth Planet. Sci. Lett.* **1996**, *142*, 43–57. [[CrossRef](#)]
 56. Normand, R.; Simpson, G.; Herman, F.; Biswas, R.H.; Bahroudi, A. Data for: Holocene sedimentary record and coastal evolution in the Makran subduction zone (Iran). *Zenodo* **2019**. [[CrossRef](#)]
 57. Bronk Ramsey, C.; Lee, S. Recent and Planned Developments of the Program OxCal. *Radiocarbon* **2013**, *55*, 720–730. [[CrossRef](#)]
 58. Reimer, P.J.; Bard, E.; Bayliss, A.; Beck, J.W.; Blackwell, P.G.; Ramsey, C.B.; Buck, C.E.; Cheng, H.; Edwards, R.L.; Friedrich, M.; et al. IntCal13 and Marine13 Radiocarbon Age Calibration Curves 0–50,000 Years cal BP. *Radiocarbon* **2013**, *55*, 1869–1887. [[CrossRef](#)]
 59. Valvo, L.M.; Murray, A.B.; Ashton, A. How does underlying geology affect coastline change? An initial modeling investigation. *J. Geophys. Res.* **2006**, *111*. [[CrossRef](#)]
 60. Limber, P.W.; Murray, A.B. Unraveling the dynamics that scale cross-shore headland relief on rocky coastlines: 2. Model predictions and initial tests. *J. Geophys. Res. Earth Surf.* **2014**, *119*, 874–891. [[CrossRef](#)]
 61. Limber, P.W.; Murray, A.B.; Adams, P.N.; Goldstein, E.B. Unraveling the dynamics that scale cross-shore headland relief on rocky coastlines: 1. Model development. *J. Geophys. Res. Earth Surf.* **2014**, *119*, 854–873. [[CrossRef](#)]
 62. Bird, E. *Coastal Geomorphology, An Introduction*; Wiley: Hoboken, NJ, USA, 2000.
 63. Ashton, A.; Murray, A.B.; Arnault, O. Formation of coastline features by large-scale instabilities induced by high-angle waves. *Nature* **2001**, *414*, 296–300. [[CrossRef](#)] [[PubMed](#)]
 64. Tamura, T. Beach ridges and prograded beach deposits as palaeoenvironment records. *Earth-Sci. Rev.* **2012**, *114*, 279–297. [[CrossRef](#)]
 65. Schwanghart, W.; Kuhn, N.J. TopoToolbox: A set of Matlab functions for topographic analysis. *Environ. Model. Softw.* **2010**, *25*, 770–781. [[CrossRef](#)]
 66. Schwanghart, W.; Scherler, D. Short Communication: TopoToolbox 2—MATLAB-based software for topographic analysis and modeling in Earth surface sciences. *Earth Surf. Dyn.* **2014**, *2*, 1–7. [[CrossRef](#)]
 67. Hurst, M.D.; Barkwith, A.; Ellis, M.A.; Thomas, C.W.; Murray, A.B. Exploring the sensitivities of crenulate bay shorelines to wave climates using a new vector-based one-line model. *J. Geophys. Res. Earth Surf.* **2015**, *120*, 2586–2608. [[CrossRef](#)]
 68. Yasso, W.E. Plan Geometry of Headland-Bay Beaches. *J. Geol.* **1965**, *73*, 702–714. [[CrossRef](#)]
 69. Axe, P.; Ilic, S.; Chadwick, A. Evaluation of beach modelling techniques behind detached breakwaters. *Coast. Eng. Proc.* **1996**, *25*, 2036–2049. [[CrossRef](#)]
 70. Otvos, E.G. Beach ridges—Definitions and significance. *Geomorphology* **2000**, *32*, 83–108. [[CrossRef](#)]
 71. Normand, R.; Simpson, G.; Herman, F.; Biswas, R.H.; Bahroudi, A.; Schneider, B. Data from: Dating and morpho-stratigraphy of uplifted marine terraces in the Makran subduction zone (Iran). *Zenodo* **2018**. [[CrossRef](#)]
 72. Schneider, B.; Hoffmann, G.; Falkenroth, M.; Grade, J. Tsunami and storm sediments in Oman: Characterizing extreme wave deposits using terrestrial laser scanning. *J. Coast. Conserv.* **2018**. [[CrossRef](#)]
 73. Plafker, G. Tectonics of the March 27, 1964 Alaska Earthquake. In *The Alaska Earthquake, March 27, 1964, Regional Effects*; U.S. Government Printing Office: Washington, DC, USA, 1966; p. 74.

74. Plafker, G.; Savage, J.C. Mechanism of the Chilean Earthquakes of May 21 and 22, 1960. *Geol. Soc. Am. Bull.* **1970**, *81*, 1001–1030. [[CrossRef](#)]
75. Sato, T.; Matsu'ura, M. Cyclic crustal movement, steady uplift of marine terraces, and evolution of the island arc-trench system in southwest Japan. *Geophys. J. Int.* **1992**, *111*, 617–629. [[CrossRef](#)]
76. Fariás, M.; Vargas, G.; Tassara, A.; Carretier, S.; Baize, S.; Melnick, D.; Bataille, K. Land-Level Changes Produced by the Mw 8.8 2010 Chilean Earthquake. *Science* **2010**, *329*, 916. [[CrossRef](#)]
77. Ota, Y.; Yamaguchi, M. Holocene coastal uplift in the western Pacific Rim in the context of late Quaternary uplift. *Quat. Int.* **2004**, *120*, 105–117. [[CrossRef](#)]
78. Pedoja, K.; Husson, L.; Johnson, M.E.; Melnick, D.; Witt, C.; Pochat, S.; Nexer, M.; Delcaillau, B.; Pinegina, T.; Poprawski, Y.; et al. Coastal staircase sequences reflecting sea-level oscillations and tectonic uplift during the Quaternary and Neogene. *Earth-Sci. Rev.* **2014**, *132*, 13–38. [[CrossRef](#)]
79. Pinegina, T.K.; Bourgeois, J.; Kravchunovskaya, E.A.; Lander, A.V.; Arcos, M.E.M.; Pedoja, K.; MacInnes, B.T. A nexus of plate interaction: Vertical deformation of holocene wave-built terraces on the kamchatsky peninsula (kamchatka, russia). *Bull. Geol. Soc. Am.* **2013**, *125*, 1554–1568. [[CrossRef](#)]
80. Wesson, R.L.; Melnick, D.; Cisternas, M.; Moreno, M.; Ely, L.L. Vertical deformation through a complete seismic cycle at Isla Santa María, Chile. *Nat. Geosci.* **2015**, *8*, 547–553. [[CrossRef](#)]
81. Simpson, G. Accumulation of permanent deformation during earthquake cycles on reverse faults. *J. Geophys. Res. Solid Earth* **2015**, *120*, 1958–1974. [[CrossRef](#)]



© 2019 by the authors. Licensee MDPI, Basel, Switzerland. This article is an open access article distributed under the terms and conditions of the Creative Commons Attribution (CC BY) license (<http://creativecommons.org/licenses/by/4.0/>).